cm CHEMISTRY OF MATERIALS

pubs.acs.org/cm Article

Anion-Directed Synthesis of Core−Shell and Janus Hybrid Nanostructures

Anchal Yadav, Bart Follink, and Alison M. Funston*

Cite This: https://doi.org/10.1021/acs.chemmater.2c02494 Read Online

ACCESS | Metrics & More | Article Recommendations | Supporting Information

ABSTRACT: Hybrid nanoparticles show considerable promise with potential applications ranging across catalysis (including photocatalysis), energy conversion, and storage. A generalized synthetic procedure for hybrid nanoparticles is presented. The method offers the flexibility to drive the products toward different hybrid nanostructure morphologies merely via a change in the metal anion, under otherwise identical experimental conditions. Both Ag@CZTS (CZTS = Cu_2ZnSnS_4) core−shell nanoparticles and Ag_2S-CZTS Janus nanoparticles, along with PbS and Au/AuAg hybrid analogues, are synthesized using this methodology, highlighting its versatility and translatability across different materials. The nucleation of the semiconductor is the critical determining step for the synthesis of a given hybrid product. Insight into the mechanism of growth for these two morphologies paves the way for the rational and generalized synthesis of hybrid nanoparticles.

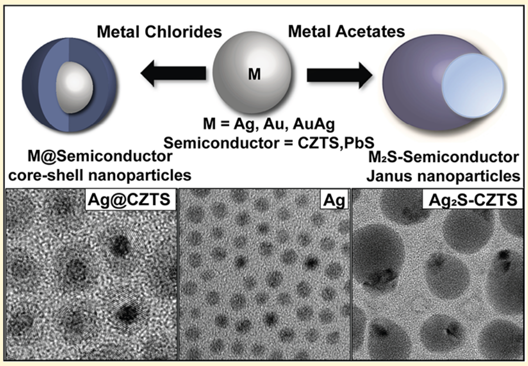

INTRODUCTION

Nanoparticles composed of different materials have the potential to combine multiple properties into a single structure as well as to access new phenomena as a consequence of the interplay between the materials or interactions at the interface. As such, they offer complementary or new properties that cannot be replicated in pure materials. This, along with their tunability and multifunctionality, has led to promising applications within photocatalysis and solar light harvesting.[1−4] Hybrid materials, incorporating both metal and semiconductor components, have shown particular efficacy in these applications. Despite this, there are very few synthetic strategies able to be applied across different metals and semiconductors to yield hybrid nanoparticles of a specific morphology.

Hybrid nanoparticles utilizing gold and semiconductors including CdS, ZnSe, CdSe, and PbS have been successfully synthesized to generate various morphologies such as Au@PbS,[5] Au@CdS,[6,7] Au-ZnSe,[8] and Au-CdSe[9] hybrid nanoparticles. These hybrids have garnered considerable attention and are widely explored as potential materials for applications such as photocatalytic water splitting and photogeneration of charge carriers.[4,10−13]

Janus structures, for example, semiconductor−semiconductor systems, display a "built-in" potential at the semiconductor−semiconductor interface. This can be exploited for the separation and transportation of photogenerated electron−hole pairs. Consequently, they can greatly improve charge separation, prevent charge recombination, and lower the overpotential for electrochemical reactions resulting in improved photocatalytic activity. Janus nanoparticles are generally synthesized using cation exchange approaches.[14−16] The process includes the diffusion of reactant atoms and exchange of ions leading to their conversion into the corresponding material, for example, the exchange of Ag^+ ions in CdS, CdSe, and CdTe nanorods generating silver chalcogenides.[17,18] Similarly, CdS−Cu_2S nanorods are formed by partial Cu^+ exchange.[19] The partial or total conversion of the primary nanocrystals depends on the stoichiometry of the reactants and experimental parameters such as growth temperature or time.[20]

Epitaxial growth of one material over the other to synthesize core-shell nanoparticles is favored by minimization of the lattice mismatch between the materials. However, the lattice mismatch is quite large for metal and semiconductor materials.[21] Plasmonic metallic gold has a lattice mismatch of almost 43% with semiconductors such as CdSe, increasing the synthetic complexity for the formation of a high-quality crystalline shell.[22] The large lattice mismatch is caused by the differences in the crystal structure and different bonding within different materials. This lattice mismatch inhibits the epitaxial growth of dissimilar materials, such as single crystalline semiconductors on metals, impeding the development of core−shell nanostructures. This is especially

Received: August 14, 2022
Revised: September 7, 2022

challenging for (quasi-) spherical core NPs with highly curved surfaces exhibiting a wide range of crystallographic facets.[21] As a result, growing semiconductor shells uniformly or epitaxially onto metals is challenging.

The high cost and scarcity of gold preclude its use in a variety of applications.[23] In contrast, silver is a potential, lower-cost, alternative. It has a higher-quality plasmon resonance compared to gold along with the advantage of its plasmon resonance being tunable into the blue region of the visible spectrum. Despite this, there are only a few reports of hybrid nanoparticles combining silver and semiconductors. There are two primary reasons for this. First, silver is less chemically inert than gold. It has high ionic mobility due to its tendency to undergo cation exchange, inhibiting the reduction of Ag^+ to its metallic state during the synthesis of hybrid particles.[24] Consequently, silver metal nanoparticles have significant potential to undergo oxidation or sulfurization.[25] Second, silver has a lattice mismatch of 50%, higher than that of gold, resulting in nonepitaxial growth and in some cases self-nucleation of the second material. Both these aspects pose challenges for the successful synthesis of core−shell nanoparticles incorporating silver, with the former being perhaps the more challenging.

Quaternary nanocrystals, such as CZTS, being nontoxic and earth-abundant, are some of the most promising materials for solar cell absorbers and photocatalysts.[26−30] The molar ratio of the three cationic precursors affects the phase composition and crystallinity of the resulting CZTS nanoparticles. Small deviations from optimal growth conditions lead to the formation of undesired phases, such as binary or ternary sulfides (for example, ZnS, Cu_2SnS_3).[31] The formation of these undesired phases not only affects the morphology and colloidal stability of the particles but also affects the electronic properties of CZTS.[32] This ultimately leads to poorer performance of the material in optoelectronic applications. Hybrid nanostructures containing CZTS semiconductor nanoparticles combined with gold to form hybrid Au@CZTS core−shell nanoparticles and Au-CZTS heterostructures have been reported.[1,29,33−36] However, tailoring the size and shape of the hybrid nanoparticles while maintaining a high yield and particle uniformity remains complex. The exploitation of the higher reactivity of silver toward sulfur to yield hybrid Janus nanostructures, combining Ag_2S with CZTS, has also been achieved.[3] Unlike the Au@CZTS synthesis,[36] this latter synthesis employs a "traditional synthesis" in the form of cation-exchange methodology in which Ag^+ ions are added to the presynthesized CZTS nanoparticles, followed by cation exchange of Zn^{2+} and Ag^+ in the CZTS lattice. The resulting nanoparticles are highly monodisperse and exhibit a significantly enhanced photocatalytic response compared to pure CZTS. Despite this progress, little is known about the formation mechanism and therefore the control of the particle morphology for these hybrid nanoparticles.

We report a generalized methodology for the synthesis of hybrid nanoparticles. The synthesis strategy drives the formation of two different morphologies via a simple cation substitution: Ag@semiconductor metal−semiconductor core−shell hybrid nanoparticles and Ag_2S−semiconductor semiconductor−semiconductor Janus nanoparticles. The method is able to be applied across different semiconductors (CZTS and PbS) and different metals (Ag, Au, and AuAg). A thorough investigation into the nucleation and growth mechanisms shows that chloride counterions play an important role in facilitating the nucleation of the semiconductor over metal nanoparticles.

■ EXPERIMENTAL SECTION

Materials. Copper(II) chloride dihydrate ($CuCl_2 \cdot 2H_2O$; 99.99%), copper(II) acetate ($Cu(OAc_2)$; 99%), zinc(II) acetate ($Zn(CH_3CO_2)_2$; 99%), zinc(II) chloride ($ZnCl_2$; 99.99%), tin(IV) acetate ($Sn(CH_3CO_2)_4$; 99.9%), tin(IV) chloride dihydrate ($SnCl_4 \cdot 2H_2O$; 99.99%), lead acetate (Pb $(CH_3COO)_2$; 99.9%), lead chloride ($PbCl_2$; 99.9%), oleylamine (OAm; 70%), octadecene (ODE; 90%), gold(III) chloride ($HAuCl_4$; 99.99%), sulfur (S; ≥99.99%), silver nitrate ($AgNO_3$; 99.8%), 1-dodecanethiol (1-DDT; 98%), *tert*-dodecanethiol (*t*-DDT; 99%), and tri-*n*-octylphosphane oxide (TOPO; 90%) were purchased from Sigma-Aldrich. Toluene and ethanol were of analytical grade and obtained from Merck. Oleylamine and octadecene were degassed and stored in a nitrogen-filled glovebox prior to use. The remaining precursors and solvents were used without further purification.

Synthesis. *Ag Nanoparticles.* The synthesis of Ag nanoparticles was modified from the reported procedure.[37] Briefly, a solution of silver nitrate (0.03 g, 0.2 mmol) in oleylamine (5.0 mL) was heated to 165 °C for 45 min under a nitrogen flow. During this time, the color of the solution changed from light yellow to dark brown, indicating the formation of silver nanoparticles. The solution was cooled down to room temperature, and the dispersion was used as seeds for the growth of semiconductor shells without further purification.

AuAg Nanoparticles. The AuAg nanoparticles were synthesized using the method reported by Wang et al.[38] In this synthesis, $AgNO_3$ (0.3 g, 2 mmol) was dissolved in octadecene (20 mL) and slowly heated to 100 °C. Separately, $HAuCl_4$ (0.03 g, 0.2 mmol) was dissolved in a mixture of oleylamine (5 mL) and octadecene (1 mL). Once the silver precursor was fully dissolved, the reduced gold solution was injected into the silver precursor solution at 100 °C. The temperature of the solution was then increased to 120 °C and held at 120 °C for 1 h. The color of the solution changed from yellow to red, indicating the formation of AuAg alloy nanoparticles. The solution was cooled down to room temperature, and ethanol (5 mL) was added. The dispersion was centrifuged at 5000 rcf for 10 min, the supernatant was discarded, and the nanocrystal precipitate was dispersed in toluene. This process was repeated twice, and the product was finally dispersed in toluene.

Au Nanoparticles. $HAuCl_4 \cdot 3H_2O$ (0.03 g, 0.2 mmol) was added to oleylamine (4.0 mL) and heated to 120 °C under a nitrogen flow for 30 min. The color of the solution changed from yellow to red, indicating the formation of gold nanoparticles. The solution was then cooled to room temperature, and ethanol (5 mL) was added. The mixture was centrifuged at 6000 rcf for 10 min, the supernatant was discarded, and the nanocrystal precipitate was dispersed in toluene.

Ag@CZTS Core−Shell Nanoparticles. Copper(II) chloride dihydrate (0.059 g, 0.35 mmol), zinc(II) chloride (0.048 g, 0.35 mmol), tin(IV) chloride dihydrate (0.088 g, 0.26 mmol), and TOPO (1 g, 2.58 mmol) were dissolved in octadecene (5.0 mL) in a three-neck round-bottom flask and degassed at 100 °C for ∼20 min. The reaction mixture was heated to 260 °C under N_2 and maintained at this temperature for 5 min, following which the temperature was reduced to 200 °C. At 200 °C, a mixture of 1-DDT (1 mL) and *t*-DDT (1 mL) was rapidly injected into the reaction flask, which led to a decrease in temperature to 165 °C. The alkylthiols were allowed to mix for 1−2 min. At 200 °C, the freshly prepared silver nanoparticles were swiftly injected, and the mixture was held at 200 °C for 60 min. The metal chloride solution changed from green to light green at 130 °C to yellow at above 150−260 °C and finally to black-brown after sulfur precursor and silver nanoparticle injection at 200 °C (Figure S1a). After 60 min, the reaction mixture was cooled to 60 °C and ethanol (3 mL) was added to precipitate the hybrid nanoparticles. The dispersion was then centrifuged at 4400 rcf for 10 min, and the supernatant was removed. The precipitate was redispersed in toluene (10 mL), and ethanol (3 mL) was added to precipitate the nanoparticles. The resulting dispersion was centrifuged at 4400 rcf for 10 min. The process was repeated twice to yield purified nanoparticles.

Ag_2S-CZTS Janus Nanoparticles. Ag_2S-CZTS Janus nanoparticles were prepared using the same method as for Ag@CZTS core−shell nanoparticles, using acetate as the counterion (i.e., in the absence of chlorides). Copper(II) acetate (0.032 g, 0.18 mmol), zinc(II) acetate (0.022 g, 0.12 mmol), tin(IV) acetate (0.024 g, 0.07 mmol), and TOPO (1 g, 2.58 mmol) were dissolved with ODE (5.0 mL) and degassed for ∼20 min at 100 °C. The reaction mixture was heated to 260 °C under N_2. The mixture was maintained at this temperature for 5 min before cooling to 200 °C. A mixture of 1-DDT (1 mL) and *t*-DDT (1 mL) was prepared separately and rapidly injected into the reaction mixture, which led to a decrease in temperature. The alkylthiols were allowed to mix for 1−2 min, and the solution was reheated to 200 °C. The freshly prepared silver nanoparticles were swiftly injected, and the mixture was held at 200 °C for 60 min. The metal acetate solution changed from blue to green at 130 °C to yellow after 180 °C and then finally to black-brown after the sulfur precursor and silver nanoparticle injection (Figure S1b). After 60 min, the reaction mixture was cooled to 60 °C and ethanol (3 mL) was added to precipitate the hybrid nanoparticles. The dispersion was centrifuged at 4400 rcf for 10 min, and the supernatant was removed. The dispersion was precipitated using ethanol as an antisolvent and toluene as a solvent. The washing cycle was repeated twice using the same procedure as previously described, and the product was finally redispersed in toluene.

Ag@PbS Core−Shell Nanoparticles. Lead chloride (0.056 g, 2 mmol), TOPO (1 g, 2.58 mmol), and octadecene (5 mL) were heated to 100 °C and degassed with N_2 for 20 min. The solution was heated to 220 °C under N_2 and cooled to 200 °C; the color of the lead precursor solution changed from white turbid to pale yellow. After 5 min, a mixture of 1-DDT (0.5 mL) and *t*-DDT (0.5 mL) was injected into the lead precursor. Just after the alkylthiol injection, the silver nanoparticles were swiftly injected into the reaction mixture and held at 200 °C for 60 min, leading to the change in color from pale yellow to black (Figure S2). After 60 min, the reaction mixture was cooled to 60 °C and ethanol (3 mL) was added to precipitate the reaction product. The dispersion was centrifuged at 4400 rcf for 10 min, and the supernatant was removed. Using ethanol as an antisolvent and toluene as a solvent, the washing procedure was repeated twice using the same procedure as previously described.

Ag_2S-PbS Janus Nanoparticles. Lead acetate (0.028 g, 1 mmol), TOPO (1 g, 2.58 mmol), and octadecene (5 mL) were heated to 100 °C and degassed with N_2 for 20 min. The solution was heated to 220 °C under N_2 and cooled to 200 °C. After 5 min at this temperature, a mixture of 1-DDT (0.5 mL) and *t*-DDT (0.5 mL) was added to the reaction solution, followed by the silver nanoparticle injection at 200 °C (Figure S2). The temperature was increased to 220 °C, and the mixture was held at 220 °C for 60 min. The solution was cooled to 60 °C. The dispersion was centrifuged at 4400 rcf for 10 min, and the supernatant was removed. The precipitate was redispersed in toluene (10 mL), and ethanol (3 mL) was added to precipitate the nanoparticles. The resulting dispersion was centrifuged at 4400 rcf for 10 min. The process was repeated twice to obtain purified nanoparticles.

AuAg@CZTS Core−Shell Nanoparticles. Copper(II) chloride dihydrate (0.059 g, 0.35 mmol), zinc(II) chloride (0.048 g, 0.35 mmol), tin(IV) chloride dihydrate (0.088 g, 0.26 mmol), and TOPO (1 g, 2.58 mmol) were dissolved in octadecene (5.0 mL) in a three-neck round-bottom flask and degassed with N_2 at 100 °C for ∼20 min. The reaction mixture was heated to 260 °C under N_2 and maintained at this temperature for 5 min over which time the color changed from light green to pale yellow to light brown. The temperature was reduced to 200 °C. At 200 °C, a mixture of 1-DDT (1 mL) and *t*-DDT (1 mL) was rapidly injected into the reaction flask. Following the DDT injection (1−2 min), the AuAg alloy nanoparticles were swiftly injected and the mixture was held at 200 °C for 30 min. After 30 min, the reaction mixture was cooled to 60 °C and the washing procedures were followed twice as described above.

Au@CZTS Core−Shell Nanoparticles. Copper(II) chloride dihydrate (0.059 g, 0.35 mmol), zinc(II) chloride (0.048 g, 0.35 mmol), tin(IV) chloride dihydrate (0.088 g, 0.26 mmol), and TOPO (1 g, 2.58 mmol) were dissolved in octadecene (5.0 mL) in a three-neck round-bottom flask and degassed at 100 °C for ∼20 min. The reaction mixture was heated to 260 °C under N_2 and maintained at this temperature for 5 min over which the color changed from light green to pale yellow to light brown. The temperature was reduced to 200 °C, and a mixture of 1-DDT (1 mL) and *t*-DDT (1 mL) was rapidly injected into the reaction flask. After DDT injection (1−2 min), the freshly prepared Au nanoparticles were swiftly injected and the mixture was held at 200 °C for 30 min. After 30 min, the reaction mixture was cooled to 60 °C and the washing procedures were followed twice as described above.

Instrumentation. Transmission electron microscopy and high-resolution transmission electron microscopy (TEM and HRTEM) were carried out using an FEI Tecnai T20 microscope with a LaB6 filament, operating at an accelerating voltage of 200 kV at room temperature. STEM images were collected using high-angle annular dark-field (HAADF) and bright-field (BF) modes with a Gatan Ultrascan 1000 high-resolution CCD camera. EDS mapping was carried out using an FEI Tecnai F20 microscope with a thermal emitter, operated at an accelerating voltage of 200 kV at room temperature. STEM images were obtained using a Gatan Ultrascan 1000 high-resolution CCD camera. The EDX signal was collected using the Bruker X-Flash X-ray detector with an energy resolution of 123 eV.

Absorption spectra were acquired on an Agilent Cary 60 UV−vis spectrometer in a 1 cm path length quartz cuvette.

X-ray diffraction (XRD) was performed using a Bruker D8 Advance diffractometer equipped with a Cu Kα (Kα = 1.54 Å) radiation source, operated at 40 kV and 40 mA. The sample was prepared by deposition of the nanoparticle dispersion onto a glass substrate. The samples were completely dried prior to measurements.

X-ray photoelectron spectroscopic (XPS) analysis was performed using a Nexsa Surface Analysis System (Thermo Fisher Scientific) with a monochromated Al-Kα source at a power of 180 W and a hemispherical analyzer operating in the fixed analyzer transmission mode. During analysis, the pressure in the main vacuum chamber was less than 10^{-8} mbar. High-resolution XPS spectra were collected at a pass energy of 200 and 50 eV and a step size of 1 and 0.1 eV, respectively.

TEM Grid Preparation. A 20 μL aliquot of the colloid was drop-casted onto the holey carbon film supported on Cu TEM grids (Ted Pella) and allowed to dry for 5 min. Following deposition, the grid was washed by rinsing with toluene to remove any organic contaminants. For STEM−EDS of copper-containing CZTS-based nanoparticles, SiN_3 grids were used to avoid the copper background for the chemical mapping of CZTS nanoparticles.

Sample Preparation for XPS. Samples were drop-casted onto a Si wafer and allowed to dry. The samples were mounted to the sample holder such that no electrical contact with the instrument ground was established.

RESULTS AND DISCUSSION

Synthesis. The generalized methodology for the synthesis of different hybrid nanoparticle morphologies across different materials is presented in Scheme 1. The formation of either core−shell or Janus nanoparticles is accomplished by considering the surface chemistry of the metallic seed and the reactivity of the copper precursor along with alkylthiols for CZTS. The reaction is driven toward one morphological product (over the other) purely by utilizing different counterions for the metal−semiconductor precursors:chloride precursors favor the formation of core−shell structures (left arrow, Scheme 1), while the use of acetates results in Janus nanoparticles (right arrow, Scheme 1).

Scheme 1. Synthetic Method Using Metal Chlorides as Counterions to Synthesize M@Semiconductor Core−Shell Nanoparticles and Metal Acetates to Synthesize M_2S−Semiconductor Janus Nanoparticles[a]

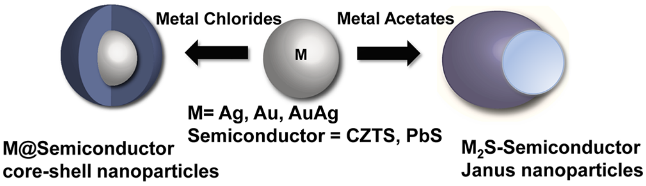

[a] The metal nanoparticles employed in this study are Ag, Au, and AuAg alloys and are represented as symbol "M", while the semiconductor used here are CZTS and PbS to generate hybrid nanoparticles. "M_2S" represents the transformation of metal to metal sulfide.

As outlined in Scheme 1, core−shell hybrid nanoparticles and Janus nanoparticles are synthesized via seed-mediated growth. Their synthesis method is essentially identical, with the only difference being the counterion of metal precursors for the semiconductor constituents. Within this method, freshly prepared metal nanoparticles are utilized as seeds. The semiconductor metal anion precursor solution, comprising metal chlorides for core−shell nanoparticles or metal acetates for Janus nanoparticles, is heated to facilitate decomposition of the precursors (260 °C for CZTS-based hybrids). Nucleation and growth of the semiconductor are initiated by the addition of the sulfur precursors (1:1 DDT: *t*-DDT), followed by the silver nanoparticle seed injection at 200 °C. The hybrid nanoparticles are grown for 60 min at 200 °C.

Representative TEM and HRTEM images showing the morphology of the resulting Ag@CZTS hybrid nanoparticles, grown in the presence of chloride counterions from Ag seeds with a diameter of 5.5 ± 1.0 nm, are shown in Figure 1a,b. The Ag@CZTS nanoparticles have regular spherical shells with good monodispersity and a morphological yield (number of particles of a given morphology/total particles) of 78% (Figure S3). The core−shell nanoparticles have a diameter of 8.1 ± 1.0 nm, with a silver core diameter of 3.9 ± 0.9 nm (size histograms in Figure S4). The growth of the CZTS shell is nonepitaxial onto the Ag core, and the shell is polycrystalline in nature. The lattice spacings measured via HRTEM and FFT are 0.29 nm, corresponding to the {101} planes of CZTS, indicative of the wurtzite phase of CZTS. The lattice plane of silver is 0.24 nm, corresponding to the {111} cubic Ag planes. The peaks observed in the XRD spectra of Ag@CZTS shown in Figure 1i are consistent with the HRTEM images, FFT pattern, and the selected area electron diffraction (SAED) pattern (Figure 1c,d). The three intense peaks observed in Ag@CZTS core−shell nanoparticles at 2θ = 38.12°, 44.30°, 64.45°, and 77.41° correspond to the 111, 200, 220, and 311 planes of cubic silver (JCPDS# 00-071-3762). The major peaks at 2θ = 26.70° (100), 28.10° (002), 30.26° (101), 47.33° (110), 51.23° (103), and 56.17° (112) are consistent with the wurtzite phase of CZTS.[39] EDS−STEM chemical mapping (Figure S5) and HAADF images (Figure S5a) show the distribution of Cu (red), Zn (green), Sn (pink), and sulfur (aqua) elements in CZTS as a concentric shell around the spherical silver core (blue), confirming the presence of a core−shell morphology. The diameter of the silver nanoparticle is reduced from the original size of the seeds (Figure S6a,b) of

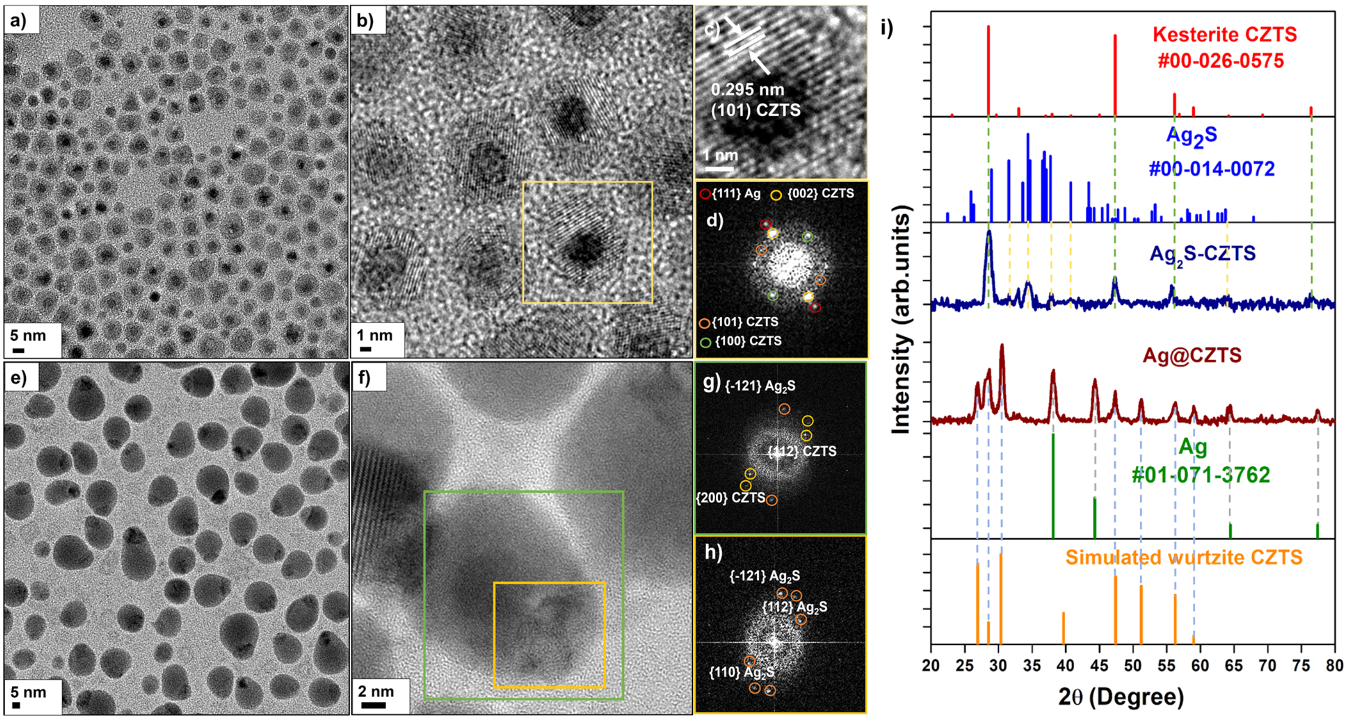

Figure 1. (a) TEM and (b, c) HRTEM images of Ag@CZTS core−shell nanoparticles in the presence of metal chlorides showing a lattice spacing of 0.295 nm corresponding to wurtzite CZTS. (d) The FFT of the marked area. (e, f) TEM and HRTEM images of Ag_2S-CZTS Janus nanoparticles synthesized in the presence of metal acetates. (g, h) The FFT of the Janus nanoparticles (marked area), showing Kesterite CZTS. (i) XRD patterns of Ag@CZTS core−shell nanoparticles (brown) and Ag_2S-CZTS Janus nanoparticles (blue) and their comparison with kesterite CZTS (JCPDS# 00-026-0575), simulated wurtzite CZTS, Ag (JCPDS# 00-071-3762), and Ag_2S (JCPDS# 00-014-0072).

https://doi.org/10.1021/acs.chemmater.2c02494

5.5 nm to 3.9 nm upon shelling. It is likely that the reduction in diameter of the metal nanoparticles after injecting into the chloride-mediated solution is due to etching caused by chloride ions in the solution. Etching of noble metal nanoparticles by halide ions has been reported[40−42] with the presence of chloride ions in Ag nanoparticle dispersions leading to dissolution of the Ag surface atoms via oxidation to AgCl.[43,44] Despite the etching, the Ag nanoparticles retain their spherical shape.

Janus nanoparticles synthesized by replacing metal chlorides with metal acetates, using an otherwise identical methodology compared to that for the core−shell nanoparticles, are shown in the TEM images in Figure 1e,f. The FFT image (Figure 1g,h) shows the {121}, {112}, and {110} Ag_2S planes, indicating that the metallic Ag seeds have transformed into semiconductor Ag_2S. Unlike enclosed core−shell nanoparticles, the morphological structure appears to be elongated, with CZTS on the one side and Ag_2S distributed at the edge of the surface of a semiconductor, yielding a CZTS-Ag_2S Janus structure. The CZTS nanoparticles are 18.2 ± 4.3 nm in diameter, while the diameter of Ag_2S is 6.6 ± 2.6 nm (size histograms; Figure S7), with a morphological yield of 94%. It is to be noted here that Ag_2S has a different contrast depending on the alignment of its crystallite *w.r.t.* the electron beam, and so some particles, which initially "appear" to have no Ag_2S, can be seen to have it in the differently tilted images (Figure S8). The Ag_2S nanoparticles in the hybrids are larger and more polydisperse than the Ag cores present in Ag@CZTS core−shell nanoparticles (Figure S9). HRTEM of Ag_2S-CZTS Janus nanoparticles shows that the polycrystalline CZTS has a lattice spacing of 0.31 nm, attributed to 112 planes of kesterite CZTS, in contrast to the wurtzite CZTS present in Ag@CZTS. Consistent with HRTEM, the major lattice spacings in the FFT pattern match kesterite CZTS (Figure 1g). XRD spectra of Ag_2S-CZTS Janus nanoparticles have (Figure 1i) peaks at $2\theta = 34.38°$ (−121), 34.70° (022), 36.80° (121), and 37.71° (−103), matching with the monoclinic crystal phase (JCPDS# 00-014-0072) of Ag_2S. Weak peaks are also observed at 40.73 and 43.40°, attributed to the 031 and 200 planes of Ag_2S. The intense CZTS peaks (JCPDS# 00-026-0575) observed at 28.53° (112), 47.33° (220), 56.17° (312), and 76.44° (332) correspond to those of the kesterite phase.[32,45] The type of capping ligands, reactivity of the precursors, and their interaction with other metal cations are known to strongly influence the crystallographic phase of CZTS.[46−49] The formation of binary sulfide ($Cu_{2-X}S$) nuclei determines the formation of wurtzite or kesterite phase. Sulfur precursors with high reactivity such as elemental sulfur generally result in the form of kesterite phase. The wurtzite CZTS phase using metal chlorides as precursors[49] (core−shell nanoparticles) is consistent with the reported CZTS phase. The EDS−STEM line scan and chemical map (Figure S10a,b) of the Janus nanoparticles show the presence of Cu, Zn, Sn, and S in the CZTS section of the nanoparticle, with Ag and S mainly distributed on the opposite side of the particle, consistent with the expected results for Janus nanoparticles. Some diffusion of silver ions into the CZTS lattice is also apparent.

The absorption spectra of Ag@CZTS and Ag_2S-CZTS in Figure 2 show that the Ag nanoparticle seeds have an intense localized surface plasmon resonance at 420 nm and CZTS nanoparticles show absorption extending into the near-infrared region. Ag@CZTS exhibits a broad absorption and a red shift in the localized surface plasmon resonance at 500−700 nm, consistent with the literature for metal−semiconductor-based core−shell nanoparticles.[6,50,51] In comparison to Ag@CZTS core−shell nanoparticles, no plasmon peak is observed in the absorption spectra of Ag_2S−CZTS Janus nanoparticles, indicating that the nanoparticles do not contain areas of pure silver metal, consistent with the silver seed becoming sulfurized to form Ag_2S.

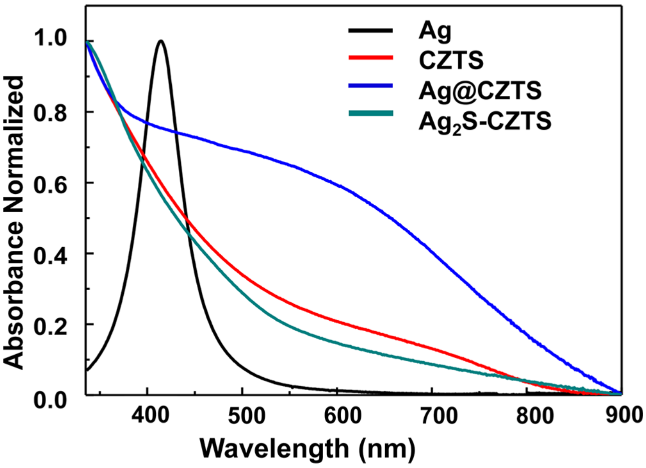

Figure 2. Absorption spectra of Ag@CZTS nanoparticles (blue), Ag_2S-CZTS Janus nanoparticles (green), and their comparison with bare Ag nanoparticles (seeds) and CZTS nanoparticles.

The elemental composition of the hybrid nanoparticle, along with oxidation states, is also consistent with the formation of core−shell and Janus particles. The average ratio of Cu/Zn/Sn/S in Ag@CZTS nanoparticles is close to 2:1:1:4, consistent with the literature.[52−54] The atomic composition determined using XPS, ICP-MS, and STEM−EDS is listed in Table S1. Some discrepancies are observed for sulfur, where the ratio of sulfur is found to be higher than predicted, particularly with ICP-MS (Table S1). This is likely because of the low signal-to-noise ratio and the lower detection limit for sulfur. Ag@CZTS nanoparticles are slightly Cu-poor, with a composition ratio of Cu/(Zn + Sn) just less than 1 (0.88; average) Sn-rich and Zn-poor, with Sn/Zn over 1 (1.27). These slight differences in CZTS stoichiometry (compared to 2:1:1:4 for Cu/Zn/Sn/S) are consistent with reports for the stoichiometry found for pure CZTS nanoparticles synthesized using chloride counter-ions.[49,55] CZTS in the Janus nanoparticles is also found to be Sn-rich or Zn-poor, as apparent from the Sn/Zn ratio (Table S1). Cu is within the stoichiometric ratio, as deduced from the ratio of Cu/(Zn + Sn) being close to 1. Janus nanoparticles are also found to have a higher composition ratio of sulfur (more than 50%). However, analysis of the average ratio of sulfur in CZTS is difficult to determine because of the presence of sulfur in both Ag_2S and CZTS nanoparticles. High-resolution X-ray photoelectron spectroscopy (XPS) shows copper, zinc, tin, and sulfide of CZTS in both core−shell nanoparticles and Janus nanoparticles to be mostly present as Cu(I), Zn(II), Sn(IV), and sulfide (Figures S11−S14). The silver core is found to be Ag(0) for the Ag@CZTS core−shell nanoparticles, whereas silver present in the Janus nanoparticle is in the form of Ag(I), consistent with silver sulfide (Figure S15). No other CZTS phase impurities are observed, except for some oxidation of Cu, Zn, and Sn which can also be observed in O1s spectra (Figure S16). Oxidation could have occurred during nanoparticle washing, sample preparation, or

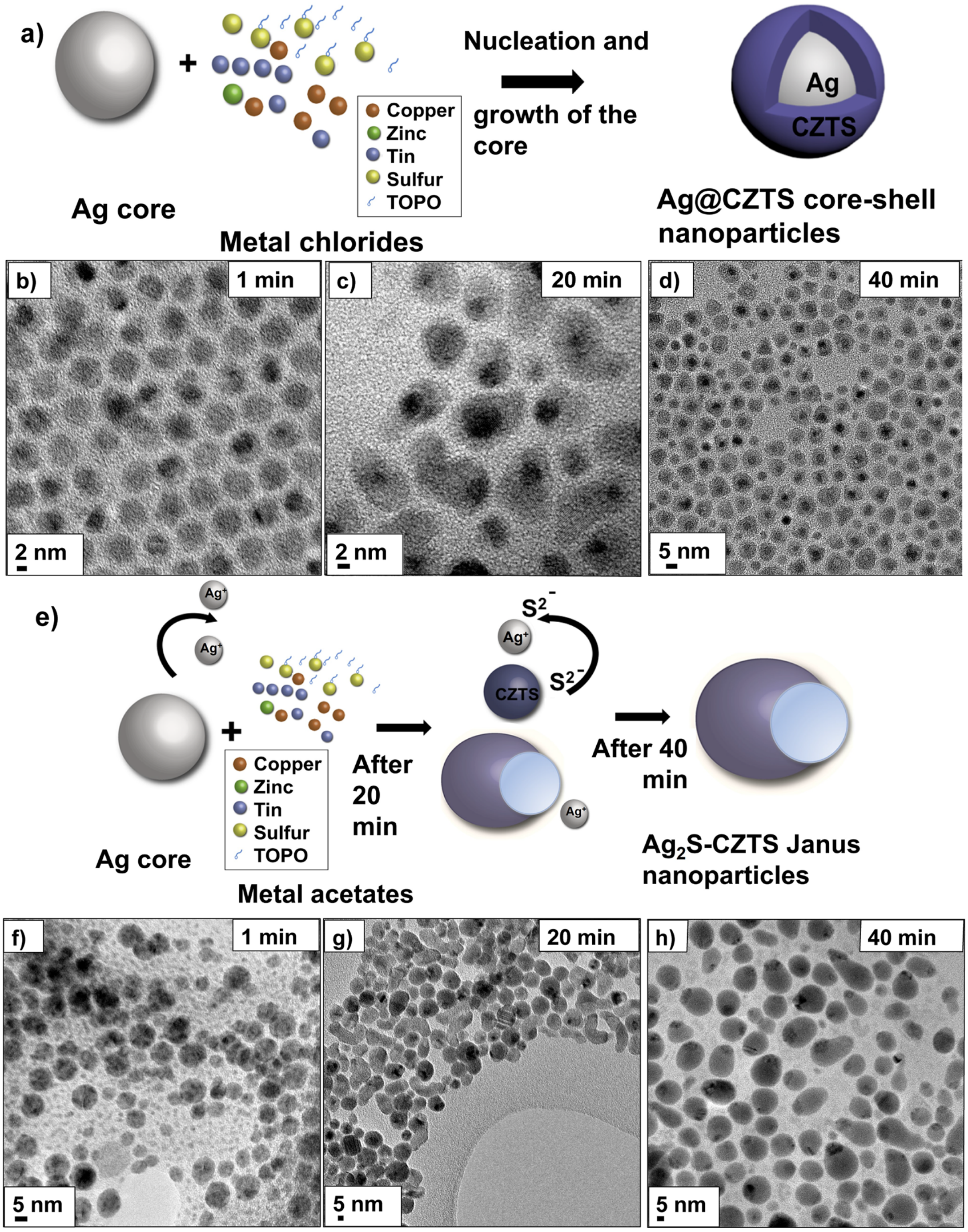

Figure 3. (a) Schematic illustration of the formation of Ag@CZTS core−shell nanoparticles with metal chlorides as precursors; TEM images of the aliquots taken during the growth process after sulfur precursor addition to the reaction solution with metal chlorides as precursors; (b) 1 min representing the core−shell nanoparticle formation; (c) 20 min and (d) after 40 min; (e) schematic illustrating the formation of Janus nanoparticles using metal acetates as precursors; and (f) 1 min, (g) 20 min, and (h) 40 min after sulfur precursor injection.

storage of the sample in ambient conditions. A list of elements and oxidation states is given in Table S2.

Reaction Mechanism. To rationalize and generalize synthetic methods for the formation of hybrid nanostructures, an understanding of the mechanistic factors governing their final morphology is required. The identity of the counterion, the differentiating factor between the formation of the different hybrid morphologies, modifies the nucleation of CZTS. Figure 3 shows TEM images of intermediate species during the reactions undertaken with different counterions. Images taken 1 min (Figure 3b) following the injection of the silver nanoparticles show that the nucleation of CZTS in the presence of chloride counterions occurs on the seeds, while in the absence of chloride ions (i.e., in the presence of acetates), CZTS self-nucleates, rather than forming on the metal nanoparticles. The scheme illustrated in Figure 3a,e describes the mechanism of formation of Ag@CZTS core−shell and Ag_2S-CZTS Janus nanoparticles. The difference in the nucleation point of the semiconductor controls the morphology of the final products, and this, in turn, is controlled by the

https://doi.org/10.1021/acs.chemmater.2c02494
Chem. Mater. XXXX, XXX, XXX−XXX

surface chemistry of the seed and reactivity of the copper precursor.

For the Ag@CZTS core−shell product after 1 min (Figure 3b), the thickness of the CZTS shells on the Ag seeds is ∼1.5−2.0 nm and the diameter of the core−shell nanoparticles is ∼4.6 nm. The silver core diameter is reduced from the seed diameter (5.5 nm) to 3.9 ± 1.8 nm. It is difficult to accurately determine the thickness of the CZTS shell due to the low crystallinity of the sample, leading to poor contrast differences in the early growth stages of the shell. At 20 min after seed injection (Figure 3c), the CZTS shells are irregular (particle diameter of ∼4.0−5.0 nm); however, they grow to yield a uniform and complete shell by 40 min, resulting in over 70% Ag@CZTS core−shell hybrid nanoparticles (Figure 3d).

When acetates are used as the counterions (Figure 3f−h), within 1 min, in contrast to that observed with chlorides as counterions, a highly polydisperse colloid is formed with a bimodal size distribution (Figure S17a). The smaller particles have a diameter of 1.2 ± 3.2 nm (Figure S17b). The population with a larger size has a diameter of 6.4 ± 1.7 nm (Figure S17c), just slightly larger than the diameter of the silver seeds (5.5 nm). At 20 min, the nanoparticles are much more uniform in size, with the smaller particles disappearing and a clear appearance of areas of different contrasts within many nanostructures. Irregularly shaped nanoparticles are also present, and the particles are relatively polydisperse. At 40 min following seed injection, Janus nanoparticles are the dominant product.

While the interpretation of the composition of the populations observed at 1 min (Figure 3f) is difficult, we suggest that the smaller nanoparticles are self-nucleated CZTS, while the larger nanoparticles are derived from the Ag seeds, which might be expected to grow in size slightly upon sulfurization. This colloid is quite different from that of the core−shell particle synthesis at 1 min (Figure 3b), which shows no evidence of small nanoparticles, consistent with the growth of a CZTS shell (as observed in the TEM at 1 min) rather than self-nucleation of the CZTS. The small particles observed in the synthesis for the Janus nanostructures have disappeared by 20 min, presumably due to further growth.

Chloride ions are known to be surface-active species with a significant propensity to adsorb onto metallic surfaces.[41,56−58] As a result, chloride ions in the solution, present as counterions from the CZTS metal precursors, would be expected to adsorb on the surface of silver nanoparticles. This surface chemistry, formed in the presence of chloride counterions, facilitates the nucleation of Cu_2S onto the seed and the growth of CZTS onto silver nanoparticles to form core−shell Ag@CZTS. When acetate precursors are used with silver seeds (from silver nitrate precursor), there is no source of chloride ion in the synthesis available for adsorption onto the seeds. This difference in surface chemistry is one factor that affects the growth mechanism (and therefore reaction products), resulting in the formation of Janus nanoparticles rather than core−shell nanoparticles when acetate counterions are used.

This hypothesis is further supported by the synthetic methods reported for Au@CZTS carried out using acetate/acetylacetonate counterions for the CZTS precursors.[36] Au seeds for Au@CZTS are synthesized from their chloride precursor, resulting in chloride ions adsorbed onto the gold nanoparticle surface prior to their injection into the CZTS precursor solution. Due to the highest chalcophilicity of Cu, it is reasonable to assume that the nucleation of $Cu_{2-X}S$ onto the metal nanoparticles should occur first for the CZTS shells, similarly to the growth of CZTS itself, followed by the incorporation of Zn and Sn into the $Cu_{2-X}S$ lattice.[32,59,60]

The higher reactivity of the $CuCl_2$ precursor relative to that of $Cu(OAc)_2$, combined with the surface chemistry of the seed, is proposed to lead to rapid adsorption of the copper (sulfide) precursor onto the seed surface. The rapid depletion of the copper precursor prevents it from becoming concentrated enough to undergo significant self-nucleation (with the sulfur precursor). In contrast, the lower reactivity of the $Cu(OAc)_2$ precursor toward the oleylamine-passivated seed (compared to those of the chloride system) allows the copper precursor to build to concentrations above the critical nucleation concentration, ultimately resulting in CZTS self-nucleation and formation of Janus hybrid nanostructures.

Syntheses using metal precursors with a combination of chloride and acetate counterions generally form core−shell morphologies,[33] although with lower yields (Figure S18c). The morphological yield of core−shell hybrid nanoparticles obtained with a mixture of Cu(II) acetate, Zn(II) acetate, and Tin(IV) chloride precursors (Figure S18c) is lower (27%) than that with all chloride precursors (shown in Table S3). Under conditions where the only chloride source is the more reactive $CuCl_2$ (compared to the acetate complex), the yield of core−shell hybrid forms remains high. This highlights the importance of rapid reduction in copper precursor concentration to prevent self-nucleation.

The formation of Ag_2S in Janus nanoparticles could be due to the diffusion of sulfur ions from CZTS into an adjoining (adsorbed) Ag nanocrystal or by sulfurization of Ag seeds prior to adsorption of Ag_2S onto the independently nucleated CZTS nanoparticles. The latter is more likely to be formed given the observed rapid initial increase in the size of the silver nanoparticle seeds. Ultimately, the Ag_2S nanocrystals are adsorbed onto the surface of CZTS, leaving a small percentage of isolated Ag/Ag_2S nanoparticles as byproducts and the Ag_2S-CZTS Janus nanoparticles with an elongated morphology as the dominant product (Figure 3h). Similar Janus nanoparticles have been synthesized by the addition of Ag^+ ions into a solution containing preformed CZTS nanoparticles,[3] and the Zn^{2+} ions are preferentially exchanged by Ag^+, generating elongated Ag_2S-CZTS Janus nanoparticles. Control experiments adding Ag^+ (in the form of $AgNO_3$), rather than the presynthesized silver nanoparticles, to presynthesized CZTS nanoparticles also show the formation of Janus particles with similar morphology (Figure S19a−c). However, the morphological yield obtained with this method is comparatively lower (53%) and the particles are more irregular than those obtained using the synthetic method with silver seeds.

The use of TOPO as the coordinating solvent in the reaction system is also found to be critical for obtaining a high yield of Ag@CZTS core−shell nanoparticles. TOPO, in general, is known to increase the crystallinity of semiconductor nanoparticles and also regulates the reactivity of metal precursors, improving sample monodispersity and achieving controlled nucleation of metal sulfides.[61,62] In the absence of TOPO, the injected DDT regulates the reactivity of metal precursors, yielding core−shell nanoparticles with a morphological yield of 40% and the remaining self-nucleated irregular CZTS nanoparticles (Figure S20b). The use of TOPO along with ODE and DDT in the reaction system enables more precise control of the particle shape, resulting in a homogeneous coating of the seeds and the formation of spherical shells, yielding 78% of

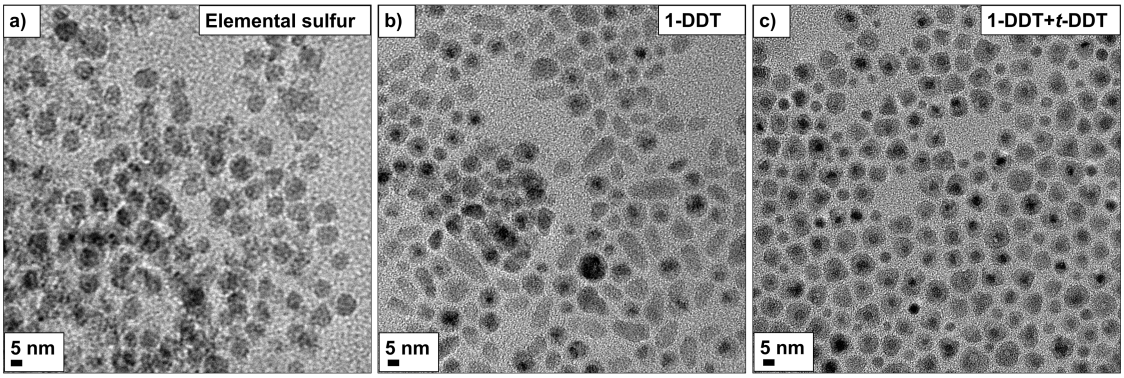

Figure 4. TEM images of the Ag@CZTS core−shell hybrid nanoparticles synthesized with (a) elemental sulfur, (b) only 1-DDT, and (c) a mixture of 1-DDT and *t*-DDT.

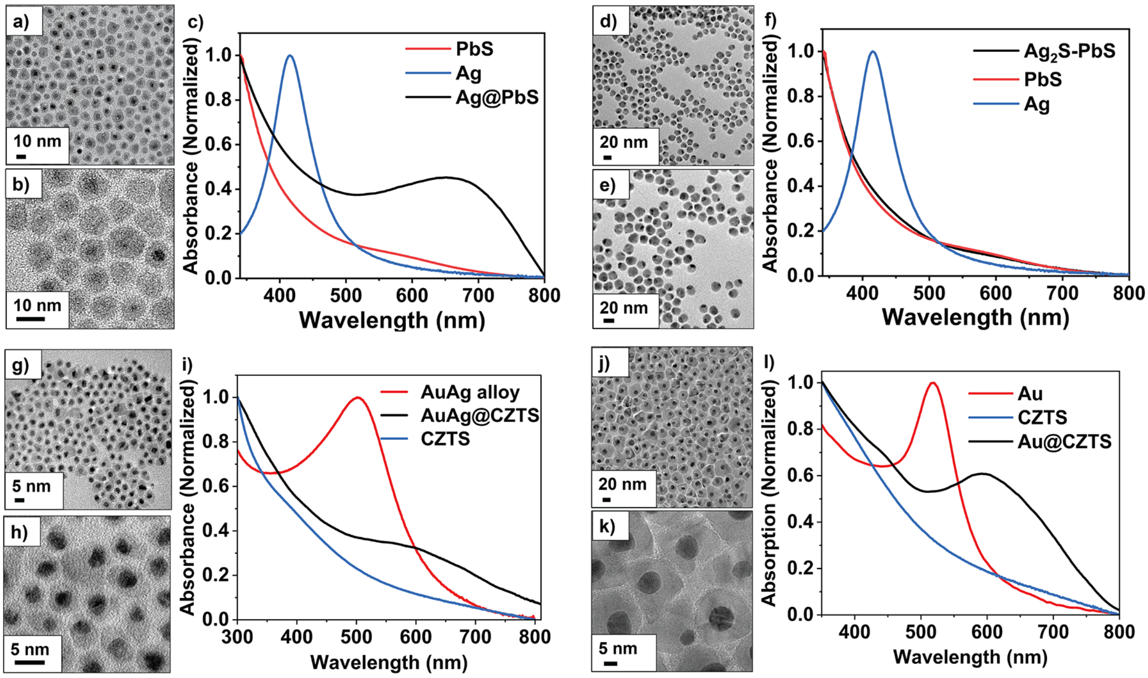

Figure 5. TEM, HRTEM, and absorption spectra of (a−c) Ag@PbS, (d−f) Ag_2S-PbS Janus nanoparticles, (g−i) AuAg@CZTS core−shell nanoparticles, and (j−l) Au@CZTS core−shell nanoparticles.

core−shell nanoparticles (Figure S20a). The synthesis of Janus nanoparticles is also carried out in the presence of TOPO; however, no changes are observed compared with those synthesized in the absence of TOPO (Figure S20c,d). This is likely due to the fact that TOPO acts as a coordinating solvent for the formation of the crystalline CZTS, which, as outlined above, for Janus particles occurs via self-nucleation due to the use of the lower reactivity of the acetate precursors.

Similarly, we have found that the use of a mixture of alkylthiols (as a source of sulfur) in the reaction solution is crucial for the formation of core−shell hybrid nanoparticles, although CZTS nanoparticles are also able to be formed using elemental sulfur and dithiocarbamates.[27,63] The morphology of the nanoparticles obtained using elemental sulfur as the sole sulfur precursor is not core−shell but instead irregular, presumably self-nucleated CZTS nanoparticles, as shown in Figure 4a. The dissolved elemental sulfur exists as an alkylammonium polysulfide, which then transforms into H_2S by reacting with excess oleylamine in the solution to generate metal sulfides much faster than alkylthiols. Alkylthiol, however, slows down the reactivity of metal precursors by forming complexes with metal ions such as metal thiolates.[64] They promote a controlled reaction important for the nucleation control of CZTS onto the Ag core, ultimately leading to core−shell nanoparticles. The 1-DDT is used as a sole sulfur precursor for the formation of chalcogenide-based disk-shaped and bullet-like morphologies.[16] It acts as both a sulfur source and a ligand, minimizing the surface area of the high-energy (112) plane and promoting the growth of (100) nanocrystal facet growth. Consistent with this, larger and irregular bullet-like nanoparticle byproducts are apparent when using 1-DDT as the sulfur source, as shown in Figure 4b, along with a low yield of core−shell hybrid nanoparticles. It is likely that the *t*-DDT has a higher chemical potential and being a more reactive counterpart of 1-DDT, the combination (1-DDT and *t*-DDT) offers the balance necessary for the formation of CZTS-based core−shell nanoparticles (Figure 4c). Similar results compared to those observed for Ag@CZTS are obtained when sulfur is used to synthesize Ag_2S-CZTS Janus nanoparticles (Figure S21a). This can be attributed to the high reactivity of the sulfur precursor toward metal precursors leading to (presumably) self-nucleation of CZTS nanoparticles. Similarly, using 1-DDT as a sole sulfur precursor yielded Janus nanoparticles along with some elongated and irregular bullet-shaped CZTS nanoparticles (Figure S21b).

The tuning and balance of reactivity of the precursors is an important aspect of the successful synthesis of core−shell particles in high yield. The results show that the higher reactivity of the copper precursor is important (along with the surface chemistry of the seed); however, this is contrasted with the mitigation of the reactivity by TOPO and the reactivity of the alkylthiol. The formation of Janus particles, which involves the sulfurization of the Ag nanoparticles, suggests that nucleation/growth of the CZTS onto Ag nanoparticles is in competition with sulfurization of the Ag nanoparticles and self-nucleation of the CZTS. The lower reactivity of the alkylthiol precursor (compared to elemental sulfur sources) moderates the rate of sulfurization of the Ag nanoparticles. It also moderates the reactivity of the metal (copper) precursors in combination with the TOPO. It can be concluded that it is a very fine balance of the reactivity of the metal, chalcogenide, and thiol precursor, combined with the surface chemistry of the seed, which drives the reaction toward the formation of core−shell nanoparticles or Janus semiconductor nanostructures.

Generalization of the Synthetic Method. There is a need for a more general synthetic approach targeted at specific hybrid morphologies. To highlight the generality of the synthetic procedure reported here across different semiconductors and metal cores, it is successfully applied to synthesize Ag@PbS core−shell nanoparticles, AuAg@CZTS core−shell nanoparticles, and Au@CZTS core−shell nanoparticles. Under the same experimental conditions, in the presence of chloride counterions and within 30 min of growth time, CZTS shells are grown onto both AuAg alloy nanoparticles and Au metal nanoparticles. Similarly, PbS shells grow onto Ag metal nanoparticles with a growth time of 60 min. As for the CZTS analogue, the synthesis of PbS shell is performed using a mixture of *t*-DDT and 1-DDT as sulfur sources, unlike pure PbS nanoparticles, which are commonly synthesized using elemental sulfur.[65−67]

TEM and HRTEM images in Figure 5 show that products obtained have a core−shell morphology with highly crystalline PbS shells, generating Ag@PbS core−shell nanoparticles with a morphological yield of 84%, AuAg@CZTS core−shell nanoparticles with a yield of 76%, and Au@CZTS core−shell nanoparticles with a yield of 88%. The HRTEM (Figure 5a,b) shows that the Ag@PbS core−shell is 8.1 ± 1.0 nm in diameter, while AuAg@CZTS is 7.8 ± 2.0 nm (Figure 5g,h) and Au@CZTS is 21.2 ± 2.0 nm (Figure 5j,k). Similar to the Ag@CZTS nanoparticles, the diameter of the AuAg core reduces slightly from 6.5 ± 1.5 to 4.3 ± 1.8 nm and for Au from 11.8 ± 1.7 to 10.5 ± 1.1 nm, while the Ag core reduces from 5.5 ± 1.0 to 3.1 ± 1.0 nm for Ag@PbS core−shell nanoparticles. The formation of PbS shells around Ag cores results in a shift of the plasmon peak from 420 nm for the Ag nanoparticles to a broad peak from 550 to 800 nm for Ag@PbS core−shell nanoparticles and 550 to750 nm for AuAg@CZTS and Au@CZTS (Figure 5c,i,l).

Ag_2S-PbS Janus nanoparticles are synthesized through nucleation of PbS from lead acetate and 1:1 DDT/*t*-DDT in the presence of silver nanoparticles, as shown in the TEM image in Figure 5d,e. The diameter of the Ag_2S particles is 5.46 ± 1.7 nm, while the diameter of PbS is 14.04 ± 3.9 nm. Similar to Ag_2S-CZTS, the absorption spectrum of the Ag_2S-PbS Janus nanoparticles, shown in Figure 5f, shows no evidence of a silver plasmon resonance, consistent with the silver becoming sulfurized.

Janus particles are not observed to form when the metallic seed contains gold, even when metal acetates are employed as the precursors for CZTS.[36] This is likely due to the presence of chloride ions in the gold precursor used for the preparation of the Au nanoparticle, $AuCl_3$.[58] Gold(III) chloride is a commonly used precursor for the synthesis of Au nanoparticles; however, using this precursor introduces chloride ions into the solution. Reproducing the synthesis of Au@CZTS core−shell nanoparticles using gold oxide for the synthesis of the gold seeds and metal acetates results in the synthesis of nanoparticles similar to Janus nanoparticles (Figure S22a,b).

■ CONCLUSIONS

We present a general strategy for the synthesis of hybrid nanoparticles of different morphologies composed of plasmonic metals (Ag, Au, and AuAg alloy) and the semiconductors CZTS and PbS. The formation of Ag@semiconductor core−shell nanoparticles is mediated by the presence of chloride ions in the solution. Chloride ions improve the nucleation of the semiconductor phase onto the surface of the metal core. Subsequent growth of the CZTS results in the formation of a core−shell morphology. The hybrid nanostructures synthesized have a nonepitaxial interface but are highly crystalline. The growth mechanism relies on finely balancing the reactivity of the metal precursors, thiol precursors, and surface chemistry of the seeds. Changing the metal precursors from chlorides to acetates, in contrast, results in the formation of Ag_2S−semiconductor Janus nanoparticles. The use of metal acetates results in the self-nucleation of CZTS as a consequence of the lower reactivity of the acetate precursors (compared with the chlorides). Silver sulfurizes in the presence of sulfur and is converted to Ag_2S, which is adsorbed on the CZTS surface forming an elongated Janus-like morphology. Understanding the mechanism of growth of these different structures combined with the ability to generalize the synthetic methodology across a range of materials is the first step in rationalizing hybrid nanostructure synthesis. This ultimately will allow the development of methods able to be applied across many metal−semiconductor combinations to achieve a specific hybrid nanocrystal morphology.

■ ASSOCIATED CONTENT

Supporting Information

The Supporting Information is available free of charge at https://pubs.acs.org/doi/10.1021/acs.chemmater.2c02494.

> Images of the reaction solutions, EDS−STEM chemical mapping and line scan of hybrid nanoparticles, size histogram of hybrid nanoparticles, TEM tilt series of Ag_2S-CZTS Janus nanoparticles, low-resolution TEM images of hybrid nanoparticles, TEM images of silver seeds, high-resolution XPS of Janus and core−shell nanoparticles, table containing the summary of binding energies of elements in core−shell and Janus nanoparticles, table containing the atom % weight composition calculation characterized by different techniques, size histograms showing particle count in 1 min of

growth solution, TEM images of Ag@CZTS core−shell hybrid nanoparticles synthesized by replacing acetates to chlorides, table containing shape yield and size of nanoparticles obtained in the presence of different counterions and TEM images of the particles utilizing the injection of Ag^+ (from $AgNO_3$) onto preformed CZTS nanoparticles, TEM images of core−shell and Janus nanoparticles synthesized in the presence and absence of TOPO, and TEM images showing Janus nanoparticles synthesized using different sulfur sources and TEM images of Janus nanoparticles synthesized using gold oxide as the gold precursor (PDF)

AUTHOR INFORMATION

Corresponding Author

Alison M. Funston − *ARC Centre of Excellence in Exciton Science and School of Chemistry, Monash University, Clayton, VIC 3800, Australia;* orcid.org/0000-0002-4320-6434; Email: alison.funston@monash.edu

Authors

Anchal Yadav − *ARC Centre of Excellence in Exciton Science and School of Chemistry, Monash University, Clayton, VIC 3800, Australia;* orcid.org/0000-0003-1307-5899

Bart Follink − *School of Chemistry, Monash University, Clayton, VIC 3800, Australia*

Complete contact information is available at: https://pubs.acs.org/10.1021/acs.chemmater.2c02494

Notes

The authors declare no competing financial interest.

ACKNOWLEDGMENTS

This work was supported by the Australian Research Council (ARC) via the ARC Centre of Excellence in Exciton Science, CE170100026. The authors acknowledge the use of facilities within the Monash Centre for Electron Microscopy (MCEM) and Monash X-ray Facilities (MXP). A.Y. also acknowledges the support from Post-graduation Publication Award (PPA) and Monash University for DIPRS and DPRS scholarships.

REFERENCES

(1) Khanal, B. P.; Pandey, A.; Li, L.; Lin, Q.; Bae, W. K.; Luo, H.; Klimov, V. I.; Pietryga, J. M. Generalized Synthesis of Hybrid Metal-Semiconductor Nanostructures Tunable from the Visible to the Infrared. *ACS Nano* **2012**, *6*, 3832−3840.

(2) Cozzoli, P. D.; Pellegrino, T.; Manna, L. Synthesis, Properties and Perspectives of Hybrid Nanocrystal Structures. *Chem. Soc. Rev.* **2006**, *35*, 1195−1208.

(3) Yu, X.; Liu, J.; Genç, A.; Ibáñez, M.; Luo, Z.; Shavel, A.; Arbiol, J.; Zhang, G.; Zhang, Y.; Cabot, A. Cu_2ZnSnS_4-Ag_2S Nanoscale p-n Heterostructures as Sensitizers for Photoelectrochemical Water Splitting. *Langmuir* **2015**, *31*, 10555−10561.

(4) Liu, X. D.; Chen, K.; Ma, S.; Hao, Z. H.; Liang, S.; Zhou, L.; Wang, Q. Q. Synthesis of Au/CdSe Janus Nanoparticles with Efficient Charge Transfer for Improving Photocatalytic Hydrogen Generation. *Nanoscale Res. Lett.* **2019**, *14*, 349.

(5) Lee, J. S.; Shevchenko, E. V.; Talapin, D. V. Au-PbS Core-Shell Nanocrystals: Plasmonic Absorption Enhancement and Electrical Doping via Intra-Particle Charge Transfer. *J. Am. Chem. Soc.* **2008**, *130*, 9673−9675.

(6) Chen, W. T.; Yang, T. T.; Hsu, Y. J. Au-CdS Core-Shell Nanocrystals with Controllable Shell Thickness and Photoinduced Charge Separation Property. *Chem. Mater.* **2008**, *20*, 7204−7206.

(7) Saunders, A. E.; Popov, I.; Banin, U. Synthesis of Hybrid CdS-Au Colloidal Nanostructures. *J. Phys. Chem. B* **2006**, *110*, 25421−25429.

(8) Bose, R.; Wasey, A. H. M. A.; Das, G. P.; Pradhan, N. Heteroepitaxial Junction in Au-ZnSe Nanostructure: Experiment versus First-Principle Simulation. *J. Phys. Chem. Lett.* **2014**, *5*, 1892−1898.

(9) Mokari, T.; Sztrum, C. G.; Salant, A.; Rabani, E.; Banin, U. Formation of Asymmetric One-Sided Metal-Tipped Semiconductor Nanocrystal Dots and Rods. *Nat. Mater.* **2005**, *4*, 855−863.

(10) Chauhan, H.; Kumar, Y.; Dana, J.; Satpati, B.; Ghosh, H. N.; Deka, S. Photoinduced Ultrafast Charge Separation in Colloidal 2-Dimensional CdSe/CdS-Au Hybrid Nanoplatelets and Corresponding Application in Photocatalysis. *Nanoscale* **2016**, *8*, 15802−15812.

(11) Wu, K.; Chen, Z.; Lv, H.; Zhu, H.; Hill, C. L.; Lian, T. Hole Removal Rate Limits Photodriven H2 Generation Efficiency in CdS-Pt and CdSe/CdS-Pt Semiconductor Nanorod-Metal Tip Heterostructures. *J. Am. Chem. Soc.* **2014**, *136*, 7708−7716.

(12) Tong, H.; Ouyang, S.; Bi, Y.; Umezawa, N.; Oshikiri, M.; Ye, J. Nano-Photocatalytic Materials: Possibilities and Challenges. *Adv. Mater.* **2012**, *24*, 229−251.

(13) Volokh, M.; Mokari, T. Metal/Semiconductor Interfaces in Nanoscale Objects: Synthesis, Emerging Properties and Applications of Hybrid Nanostructures. *Nanoscale Adv.* **2020**, *2*, 930−961.

(14) Jain, P. K.; Amirav, L.; Aloni, S.; Alivisatos, A. P. Nanoheterostructure Cation Exchange: Anionic Framework Conservation. *J. Am. Chem. Soc.* **2010**, *132*, 9997−9999.

(15) Chauhan, A.; Rastogi, M.; Scheier, P.; Bowen, C.; Kumar, R. V.; Vaish, R. Janus Nanostructures for Heterogeneous Photocatalysis. *Appl. Phys. Rev.* **2018**, *5*, No. 041111.

(16) Xia, C.; Van Oversteeg, C. H. M.; Bogaards, V. C. L.; Spanjersberg, T. H. M.; Visser, N. L.; Berends, A. C.; Meeldijk, J. D.; De Jongh, P. E.; De Mello Donega, C. Synthesis and Formation Mechanism of Colloidal Janus-Type $Cu_{2-X}S/CuInS_2$ Heteronanorods via Seeded Injection. *ACS Nano* **2021**, *15*, 9987−9999.

(17) Liu, M.; Zeng, H. C. General Synthetic Approach to Heterostructured Nanocrystals Based on Noble Metals and I-VI, II-VI, and I-III-VI Metal Chalcogenides. *Langmuir* **2014**, *30*, 9838−9849.

(18) Dong, H. S.; Hughes, S. M.; Yin, Y.; Alivisatos, A. P. Cation Exchange Reactions in Ionic Nanocrystals. *Science* **2004**, *306*, No. 1103755.

(19) Sadtler, B.; Demchenko, D. O.; Zheng, H.; Hughes, S. M.; Merkle, M. G.; Dahmen, U.; Wang, L. W.; Alivisatos, A. P. Selective Facet Reactivity during Cation Exchange in Cadmium Sulfide Nanorods. *J. Am. Chem. Soc.* **2009**, *131*, 5285−5293.

(20) Steimle, B. C.; Fagan, A. M.; Butterfield, A. G.; Lord, R. W.; McCormick, C. R.; Di Domizio, G. A.; Schaak, R. E. Experimental Insights into Partial Cation Exchange Reactions for Synthesizing Heterostructured Metal Sulfide Nanocrystals. *Chem. Mater.* **2020**, *32*, 5461−5482.

(21) Liu, J.; Zhang, J. Nanointerface Chemistry: Lattice-Mismatch-Directed Synthesis and Application of Hybrid Nanocrystals. *Chem. Rev.* **2020**, *120*, 2123−2170.

(22) Zhang, J.; Tang, Y.; Lee, K.; Ouyang, M. Nonepitaxial Growth of Hybrid Core-shell Nanostructures with Large Lattice Mismatches. *Science* **2010**, *327*, 1634−1638.

(23) Liu, L.; Zhang, X.; Yang, L.; Ren, L.; Wang, D.; Ye, J. Metal Nanoparticles Induced Photocatalysis. *Natl. Sci. Rev.* **2017**, *4*, 761−780.

(24) Beberwyck, B. J.; Surendranath, Y.; Alivisatos, A. P. Cation Exchange: A Versatile Tool for Nanomaterials Synthesis. *J. Phys. Chem. C* **2013**, *117*, 19759−19770.

(25) Liu, H.; Ye, F.; Cao, H.; Ji, G.; Lee, J. Y.; Yang, J. A Core−Shell Templated Approach to the Nanocomposites of Silver Sulfide and Noble Metal Nanoparticles with Hollow/Cage-Bell Structures. *Nanoscale* **2013**, *5*, 6901−6907.

(26) Ramasamy, K.; Malik, M. A.; O'Brien, P. Routes to Copper Zinc Tin Sulfide Cu_2ZnSnS_4 a Potential Material for Solar Cells. *Chem. Commun.* **2012**, *48*, 5703−5714.

(27) Guo, Q.; Hillhouse, H. W.; Agrawal, R. Synthesis of Cu_2ZnSnS_4 Nanocrystal Ink and Its Use for Solar Cells. *J. Am. Chem. Soc.* **2009**, *131*, 11672−11673.

(28) Zhou, H.; Hsu, W. C.; Duan, H. S.; Bob, B.; Yang, W.; Song, T. Bin.; Hsu, C. J.; Yang, Y. CZTS Nanocrystals: A Promising Approach for next Generation Thin Film Photovoltaics. *Energy Environ. Sci.* **2013**, *6*, 2822−2838.

(29) Ganai, A.; Maiti, S. P.; Houben, L.; Bar-Ziv, R.; Sadan, B. M. Inside-Out:The Role of Buried Interfaces in Hybrid Cu_2ZnSnS_4− Noble Metals. *J. Phys. Chem. C* **2017**, *12*, 7062−7068.

(30) Aldakov, D.; Lefrancois, A.; Reiss, P. Ternary and Quaternary Metal Chalcogenide Nanocrystals: Synthesis, Properties and Applications. *J. Mater. Chem. C* **2013**, *1*, 3756−3776.

(31) Yu, X.; Shavel, A.; An, X.; Luo, Z.; Ibáñez, M.; Cabot, A. Cu_2ZnSnS_4-Pt and Cu_2ZnSnS_4-Au Heterostructured Nanoparticles. *J. Am. Chem. Soc.* **2014**, *136*, 9236−9239.

(32) Zhou, B.; Xia, D.; Wang, Y. Phase-Selective Synthesis and Formation Mechanism of CZTS Nanocrystals. *RSC Adv.* **2015**, *5*, 70117−70126.

(33) Patra, B. K.; Shit, A.; Guria, A. K.; Sarkar, S.; Prusty, G.; Pradhan, N. Coincident Site Epitaxy at the Junction of Au-Cu_2ZnSnS_4 Heteronanostructures. *Chem. Mater.* **2015**, *27*, 650−657.

(34) Ha, E.; Yoon, L.; Lee, S.; Wang, J.; Li, F.; Wong, K. Signifi Cant Enhancement in Photocatalytic Reduction of Water to Hydrogen by Au/Cu_2ZnSnS_4 Nanostructure. *Adv. Mater.* **2014**, *26*, 3496−3500.

(35) Dilsaver, P. S.; Reichert, M. D.; Hallmark, B. L.; Thompson, M. J.; Vela, J. Cu_2ZnSnS_4-Au Heterostructures: Toward Greener Chalcogenide-Based Photocatalysts. *J. Phys. Chem. C* **2014**, *118*, 21226−21234.

(36) Zhang, X.; Wu, X.; Centeno, A.; Ryan, M. P.; Alford, N. M.; Riley, D. J.; Xie, F. Significant Broadband Photocurrent Enhancement by Au-CZTS Core-Shell Nanostructured Photocathodes. *Sci. Rep.* **2016**, *6*, No. 23364.

(37) Chen, M.; Feng, Y. G.; Wang, X.; Li, T. C.; Zhang, J. Y.; Qian, D. J. Silver Nanoparticles Capped by Oleylamine: Formation, Growth, and Self-Organization. *Langmuir* **2007**, *23*, 5296−5304.

(38) Wang, C.; Yin, H.; Chan, R.; et al. One-Pot Synthesis of Oleylamine Coated AuAg Alloy NPs and Their Catalysis for CO Oxidation. *Chem. Mater.* **2009**, *21*, 433−435.

(39) Lu, X.; Zhuang, Z.; Peng, Q.; Li, Y. Wurtzite Cu_2ZnSnS_4 Nanocrystals: A Novel Quaternary Semiconductor. *Chem. Commun.* **2011**, *47*, 3141−3143.

(40) Boles, M. A.; Ling, D.; Hyeon, T.; Talapin, D. V. The Surface Science of Nanocrystals. *Nat. Mater.* **2016**, *15*, 141−153.

(41) Heuer-Jungemann, A.; Feliu, N.; Bakaimi, I.; Hamaly, M.; Alkilany, A.; Chakraborty, I.; Masood, A.; Casula, M. F.; Kostopoulou, A.; Oh, E.; Susumu, K.; Stewart, M. H.; Medintz, I. L.; Stratakis, E.; Parak, W. J.; Kanaras, A. G. The Role of Ligands in the Chemical Synthesis and Applications of Inorganic Nanoparticles. *Chem. Rev.* **2019**, *119*, 4819−4880.

(42) Ghosh, S.; Manna, L. The Many "Facets" of Halide Ions in the Chemistry of Colloidal Inorganic Nanocrystals. *Chem. Rev.* **2018**, *118*, 7804−7864.

(43) Yoo, J.; So, H.; Yang, M. H.; Lee, K. J. Effect of Chloride Ion on Synthesis of Silver Nanoparticle Using Retrieved Silver Chloride as a Precursor from the Electronic Scrap. *Appl. Surf. Sci.* **2019**, *475*, 781−784.

(44) Levard, C.; Mitra, S.; Yang, T.; Jew, A. D.; Badireddy, A. R.; Lowry, G. V.; Brown, G. E. Effect of Chloride on the Dissolution Rate of Silver Nanoparticles and Toxicity to E. Coli. *Environ. Sci. Technol.* **2013**, *47*, 5738−5745.

(45) Camara, S. M.; Wang, L.; Zhang, X. Easy Hydrothermal Preparation of Cu_2ZnSnS_4 (CZTS) Nanoparticles for Solar Cell Application. *Nanotechnology* **2013**, *24*, No. 495401.

(46) Chen, K.; Zhou, J.; Chen, W.; Zhong, Q.; Yang, T.; Yang, X.; Deng, C.; Liu, Y. Growth Kinetics and Mechanisms of Multinary Copper-Based Metal Sulfide Nanocrystals. *Nanoscale* **2017**, *9*, 12470−12478.

(47) Thompson, M. J.; Ruberu, T. P. A.; Blakeney, K. J.; Torres, K. V.; Dilsaver, P. S.; Vela, J. Axial Composition Gradients and Phase Segregation Regulate the Aspect Ratio of Cu_2ZnSnS_4 Nanorods. *J. Phys. Chem. Lett.* **2013**, *4*, 3918−3923.

(48) Yang, Y.; Ding, Y.; Zhang, J.; Liang, N.; Long, L.; Liu, J. Insight into the Growth Mechanism of Mixed Phase CZTS and the Photocatalytic Performance. *Nanomaterials* **2022**, *12*, 1439.

(49) Shavel, A.; Ibáñez, M.; Luo, Z.; De Roo, J.; Carrete, A.; Dimitrievska, M.; Gencì, A.; Meyns, M.; Pérez-Rodríguez, A.; Kovalenko, M. V.; Arbiol, J.; Cabot, A. Scalable Heating-Up Synthesis of Monodisperse Cu_2ZnSnS_4 Nanocrystals. *Chem. Mater.* **2016**, *28*, 720−726.

(50) Zeng, J.; Huang, J.; Liu, C.; Wu, C. H.; Lin, Y.; Wang, X.; Zhang, S.; Hou, J.; Xia, Y. Gold-Based Hybrid Nanocrystals through Heterogeneous Nucleation and Growth. *Adv. Mater.* **2010**, *22*, 1936−1940.

(51) Lu, W.; Wang, B.; Zeng, J.; Wang, X.; Zhang, S.; Hou, J. G. Synthesis of Core/Shell Nanoparticles of Au/CdSe via Au-Cd Bialloy Precursor. *Langmuir* **2005**, *21*, 3684−3687.

(52) Tiong, V. T.; Bell, J.; Wang, H. One-Step Synthesis of High Quality Kesterite Cu_2ZnSnS_4 Nanocrystals - a Hydrothermal Approach. *Beilstein J. Nanotechnol.* **2014**, *5*, 438−446.

(53) Zou, Y.; Su, X.; Jiang, J. Phase-Controlled Synthesis of Cu_2ZnSnS_4 Nanocrystals: The Role of Reactivity between Zn and S. *J. Am. Chem. Soc.* **2013**, *135*, 18377−18384.

(54) Sarswat, P. K.; Free, M. L. An Investigation of Rapidly Synthesized Cu_2ZnSnS_4 Nanocrystals. *J. Cryst. Growth* **2013**, *372*, 87−94.

(55) Ahmad, R.; Saddiqi, N. U. H.; Wu, M.; Prato, M.; Spiecker, E.; Peukert, W.; Distaso, M. Effect of the Counteranion on the Formation Pathway of Cu_2ZnSnS_4 (CZTS) Nanoparticles under Solvothermal Conditions. *Inorg. Chem.* **2020**, *59*, 1973−1984.

(56) Lohse, S. E.; Burrows, N. D.; Scarabelli, L.; Liz-Marzán, L. M.; Murphy, C. J. Anisotropic Noble Metal Nanocrystal Growth: The Role of Halides. *Chem. Mater.* **2014**, *26*, 34−43.

(57) Juarez, B. H. The Role of Halogens in the Synthesis of Semiconductor Nanocrystals. *Z. Phys. Chem.* **2015**, *229*, 119−137.

(58) Hinrichs, D.; Galchenko, M.; Kodanek, T.; Naskar, S.; Bigall, N. C.; Dorfs, D. Chloride Ion Mediated Synthesis of Metal/Semiconductor Hybrid Nanocrystals. *Small* **2016**, *12*, 2588−2594.

(59) Liao, H. C.; Jao, M. H.; Shyue, J. J.; Chen, Y. F.; Su, W. F. Facile Synthesis of Wurtzite Copper-Zinc-Tin Sulfide Nanocrystals from Plasmonic Djurleite Nuclei. *J. Mater. Chem. A* **2013**, *1*, 337−341.

(60) Yarur Villanueva, F.; Green, P. B.; Qiu, C.; Ullah, S. R.; Buenviaje, K.; Howe, J. Y.; Majewski, M. B.; Wilson, M. W. B. Binary $Cu_{2-X}S$ Templates Direct the Formation of Quaternary Cu_2ZnSnS_4 (Kesterite, Wurtzite) Nanocrystals. *ACS Nano* **2021**, *15*, 18085−18099.

(61) Riha, S. C.; Parkinson, A. B.; Prieto, K. A. Solution-Based Synthesis and Characterization of Cu_2ZnSnS_4 Nanocrystals. *J. Am. Chem. Soc.* **2009**, *131*, 12054−12055.

(62) Wang, F.; Tang, R.; Buhro, W. E. The Trouble with TOPO; Identification of Adventitious Impurities Beneficial to the Growth of Cadmium Selenide Quantum Dots, Rods, and Wires. *Nano Lett.* **2008**, *8*, 3521−3524.

(63) Liu, K.; Yao, B.; Li, Y.; Ding, Z.; Sun, H.; Jiang, Y.; Wang, G.; Pan, D. A Versatile Strategy for Fabricating Various Cu_2ZnSnS_4 Precursor Solutions. *J. Mater. Chem. C* **2017**, *5*, 3035−3041.

(64) Tan, J. M. R.; Lee, Y. H.; Pedireddy, S.; Baikie, T.; Ling, X. Y.; Wong, L. H. Understanding the Synthetic Pathway of a Single-Phase Quarternary Semiconductor Using Surface-Enhanced Raman Scattering: A Case of Wurtzite Cu_2ZnSnS_4 Nanoparticles. *J. Am. Chem. Soc.* **2014**, *136*, 6684−6692.

(65) Liu, J.; Yu, H.; Wu, Z.; Wang, W.; Peng, J.; Cao, Y. Size-Tunable near-Infrared PbS Nanoparticles Synthesized from Lead Carboxylate and Sulfur with Oleylamine as Stabilizer. *Nanotechnology* **2008**, *19*, No. 345602.

(66) Yuan, B.; Egner, T. K.; Venditti, V.; Cademartiri, L. Sustainable Scalable Synthesis of Sulfide Nanocrystals at Low Cost with an Ionic Liquid Sulfur Precursor. *Nat. Commun.* **2018**, *9*, No. 4078.

(67) Joo, J.; Na, B. H.; Yu, T.; Yu, H. J.; Kin, W. Y.; Wu, F.; Zhang, Z. J.; Hyeon, T. Generalized and Facile Synthesis of Semiconducting Metal Sulfide Nanocrystals. *J. Am. Chem. Soc.* **2003**, *125*, 11100−11105.

https://doi.org/10.1021/acs.chemmater.2c02494